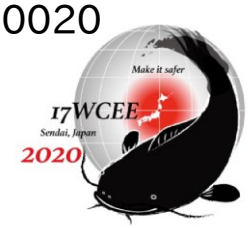

17th World Conference on Earthquake Engineering, 17WCEE
Sendai, Japan - September 13th to 18th 2020

COUPLED EFFECTIVE STRESS ANALYSIS OF SAND LIQUEFACTION FOR PETOBO SITE POST M_W 7.4 PALU EARTHQUAKE

I.W. Sengara[(1)], A. Sulaiman[(2)], L.E. Widodo[(3)]

[(1)] *Professor, Faculty of Civil and Environment Engineering, Institut Teknologi Bandung, Indonesia*
[(2)] *Research Assistant, Faculty of Civil and Environment Engineering, Institut Teknologi Bandung, Indonesia*
[(3)] *Associate Professor, Faculty of Mining and Mineral Engineering, Institut Teknologi Bandung, Indonesia*

Abstract

Ground failures generated by liquefaction had been a major cause of damages in Indonesia during past earthquakes among others: 2006 Yogyakarta, 2009 Padang, and 2018 Palu earthquake. Estimating deformations due to seismically induced liquefaction is often accomplished with a series of simplified analyses. An alternative approach adopting coupled effective stress analysis is presented in this paper to estimate liquefaction-induced flow failure in the effort to provide improvement in the deformations prediction. The method is adopted for the liquefaction slope occurrence during 2018 Palu earthquake. In order to assess the liquefaction potential and analyze the seismic deformation response of the slope, subsurface exploration has been carried out in several liquefied sites. The Palu liquefaction occurrence was also identified to be contributed by aquifer existence beneath the liquefied layer. This liquefaction of the sand layers in combination with the aquifer pressure under high seismic excitation contributes to the flow liquefaction that travel long distance which has damaged many houses along the critical zones in Petobo, Jono Oge, and Balaroa. Numerical analyses adopting effective stress method coupled with the aquifer pressure were carried out to verify the liquefaction occurrence. An effective stress dynamic analyses were carried out using FLAC2D version 7.0 (Itasca, 2011) utilizing UBCSAND constitutive model. Additionally, the large-strain mode is applied to calculate liquefaction-induced flow failure. The proposed approach can be used both for post-earthquake evaluations and for pre-earthquake vulnerability predictions on others area.

Keywords: Liquefaction; dynamic analysis; effective stress method; finite difference method; Palu Earthquake

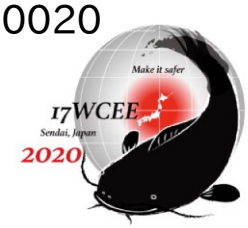

1. Introduction

Earthquake shaking may trigger the liquefaction of a saturated sandy soil in the ground. After being recognized the liquefaction phenomenon during the 1964 Great Niigata and Alaska earthquakes, many researches have been conducted concerning liquefaction in different parts of the world. Recently, researches are being conducted to estimate liquefaction-induced lateral ground displacements including numerical models, laboratory tests, and field-test-based methods. A rely on variations of the Newmark integration procedure might be used for estimating the liquefaction-induced lateral displacement. There are many advantages to this analytical technique including simplicity of input and procedure and the relative ease in understanding the assumptions and predictions. But for thoroughly understanding the response of sandy soil to cyclic shear loads, numerical modeling technique is better. Predicting the response of liquefiable soil behavior during an earthquake is highly dependent on adequately accounting for the effects of pore water pressure development, stress-strain softening and shear strength reduction behavior. The effective stress method is a useful tool in modeling the generation of pore water pressure, stress-strain behavior and degradation of soil strength.

In this study, a coupled effective stress analysis is demonstrated using finite-difference method. The method is performed through to the seismic slope behavior in Palu, Indonesia due to Palu Earthquake. Previously, Sengara et al. (2019) conducted a series of two dimensional effective stress dynamic analyses in order to study the deformation of slope in Petobo, Palu, Indonesia. The analyses indicated that the Petobo slopes deformed in excess of 16 m. In order to evaluate soil behavior during earthquake so that the deformation is closer compared to the satellite observation, some additional findings are modeled from the latest observation such as clay and water film layer which is found between 1 and 2-meter depth, additional pore pressure due to cracking confined aquifer at a depth of about 30 meter below ground surface, and additional soil characterization from the latest soil investigation. However, the detail of earthquake description and post-earthquake site survey can be learned at published paper Sengara et al. (2019) [11].

The back calculation of flow liquefaction in liquefied zone was performed using finite-difference method. A non-linear effective stress analysis was used to evaluate soil behavior during time utilizing UBCSAND constitutive model. This study can be used both for post-earthquake evaluations and for pre-earthquake vulnerability predictions.

2. Numerical Modeling Procedure

In this study, a two-dimensional (2D) reference model is developed to simulate seismic behavior of a slope in Petobo, Palu, Indonesia. Nonlinear time history dynamic analysis is carried out using computer program FLAC 2D. This program is based on a continuum finite difference discretization using the Lagrangian approach. For dynamic analysis, it uses an explicit finite difference scheme to solve the full equation of motion using lumped grid point masses derived from the real density surrounding zone.

In this analysis, the UBCSAND model is utilized and used to conduct coupled effective stress dynamic analysis which take into account the effects of seismically induced pore water pressures to investigate the degree of liquefaction.

Firstly, a static analysis considering the effect of gravity with the Mohr-Coulomb elastic perfectly plastic constitutive model is performed to establish the in-situ stresses before seismic loading. The water within the soil is modeled directly and is allowed to flow during the static solutions. Static solutions are obtained by including damping terms that gradually remove kinetic energy from the system. Once initial stress state is established in the model and the soil model changed, the effective stress dynamic analysis is started. During the dynamic solutions, excess pore water pressure is allowed to generate and also the dissipation of these pore pressures is modelled. This effective stress analysis which takes into account the effects of seismically induced pore water pressures is used to investigate the degree of liquefaction which is occurred in slope area. It should be noted that, all analyses are performed under fully drained condition. One

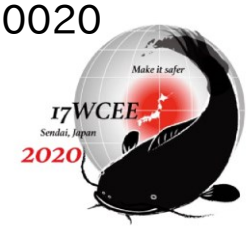

key advantage of the coupled numerical approach is the ability to account for the interdependent effects of various mechanisms and phenomena on each other as the numerical computations proceed. For instance, when an effective stress formulation is used, the inclusion of pore water pressure generation in the simulation can impact the strength and stress-strain behavior of the soil during earthquake in the same manner as in the field.

In this study, the large-strain mode is applied to calculate liquefaction-induced flow failure. In large-strain mode, the orientation θ of the weak plane is adjusted continuously, per zone, to account for rigid body rotations due to deformations. It means the stresses at time (t + Δt) is corrected incrementally by the stress-rotation correction. Figure 1 illustrates the weak plane of mesh, global axis (x,y), and local (x',y') coordinate frames.

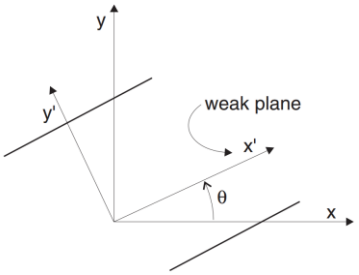

Fig. 1 A Weak Plane Oriented at an Angle θ to the Global Reference Frame

3. Characteristic of The Seismic Event

The study was carried out at the slope in Petobo, Palu, Indonesia observed lateral flow failure reach a total about hundreds meter. This analysis intends to reproduce the incidences submitted during The Palu earthquake (Mw 7,4) on September 28, 2019. The epicenter earthquake located at 0.18°N and 119.85°W in the Central Sulawesi. The epicenter was approximately 72 km north of Palu City at a depth of 10 km associated with the Palu-Koro fault line Donggala, Central Sulawesi, Indonesia.

The Palu-Koro fault zone separates the Sulawesi Sea from the Makassar Basin, dividing it into the North Makassar and South Makassar Basins. The Palu-Koro transform fault caused part of western Sulawesi to move in a south-southeasterly direction, which influenced the island's position and caused two small spreading centers in the Makassar Strait to become dormant.

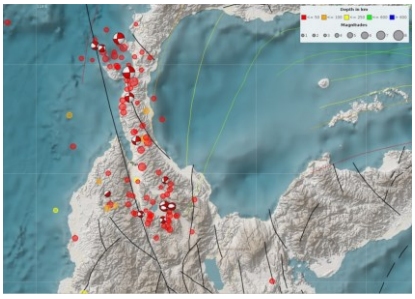

(a)

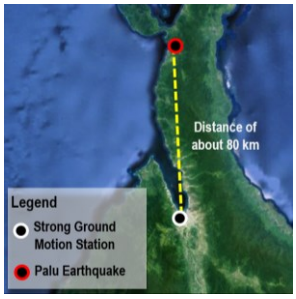

(b)

Fig. 2 (a) Aftershock Distribution within 4 days after Palu Earthquake Occurred (GEMPA, 2018) and (b) Location of Strong Ground Motion Station Corresponding to Palu Earthquake

This major tremor was preceded by a series of small-to-moderate sized earthquakes over the hours leading up to this event; the USGS located 4 other earthquakes of M 4.9 and larger in the epicentral region, beginning with a M 6.1 earthquake three hours earlier and just to the south of the M 7.4 event. There has also been an active aftershock sequence, with 40 events of M 4.4 and larger in the first five days following this earthquake.

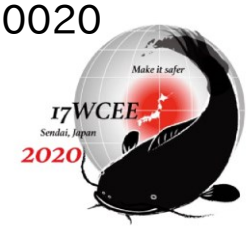

The closest strong ground motion PCI-PALU (BMKG-JICA) station was located at 0.91°S and 119.84°E (80 km to the south of the epicenter) and recorded the PGAs of about 0.281g in the East-West direction, 0.203g in the North-South direction, and 0.335g in the Up-Down (vertical) direction. The acceleration time histories of the recorded ground motion caused by the Palu Earthquake event and location of ground motion station are illustrated in Figure 2b and 3, respectively.

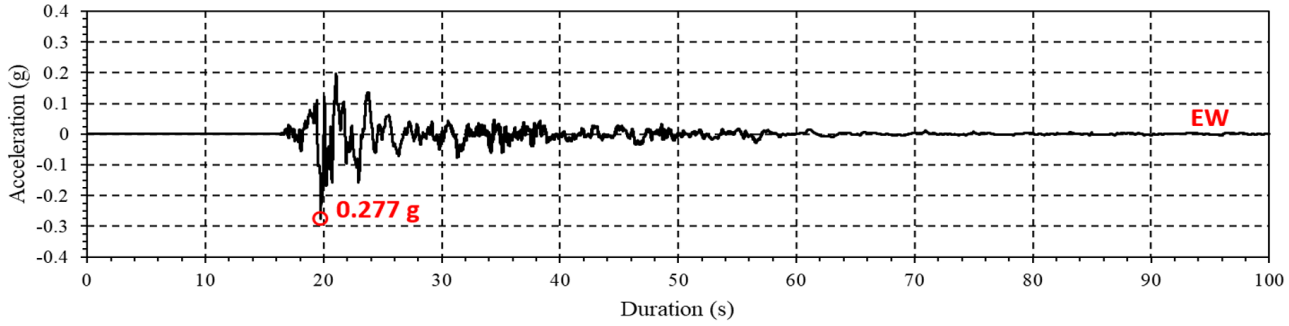

(a)

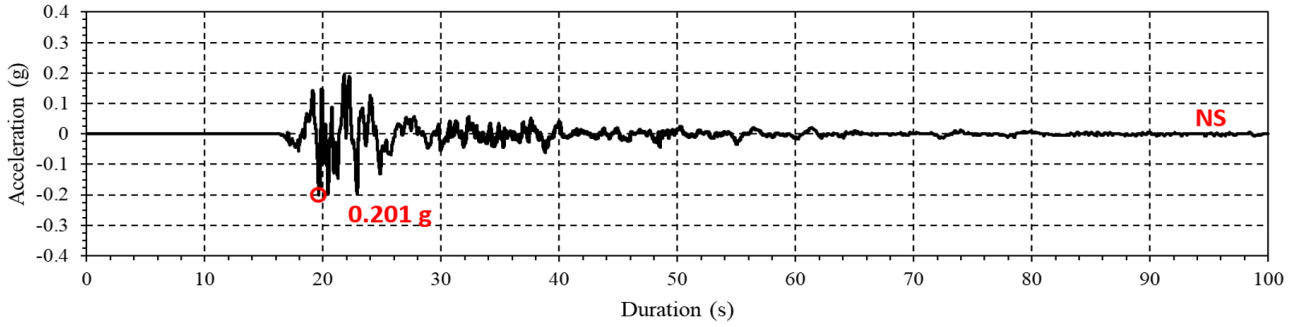

(b)

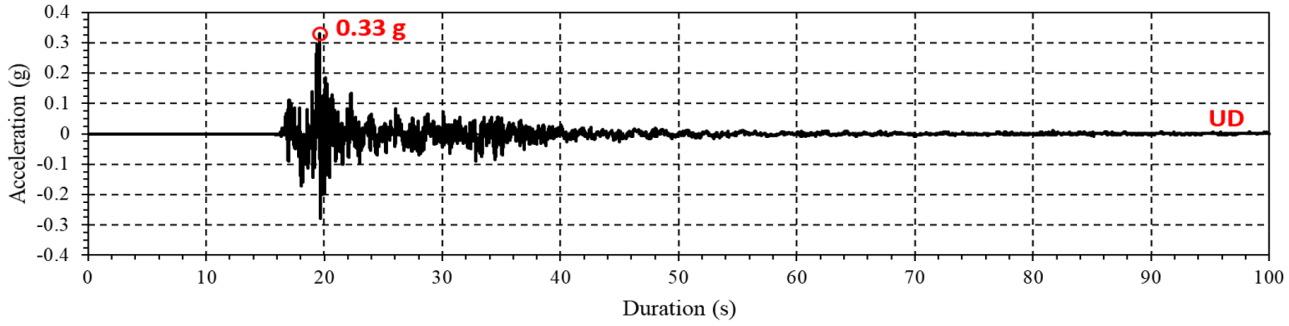

(c)

Fig. 3 – Ground Motions of Palu Earthquake from PCI-PALU Stations (a) E-W Direction, (b) N-S Direction and (c) U-D Direction (BMKG-JICA, 2019)

4. Post Earthquake Site Survey

A number of documentations by the authors on the Petobo, Palu, Indonesia showed the phenomenon of flow liquefaction and widespread nature from earthquakes in this region. Some buildings, roads, and slopes moved with very large deformations and caused the road and bridge collapsed (Figure 4c and Figure 4d).

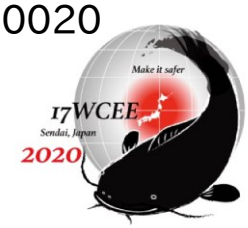

The Petobo flow-slide is located approximately 1 km south of the Palu and the total area of the slide is approximately 1.5 km^2 covering the source, runout, and deposition zones. There was several ponding water that develop on site with unknown water source in Petobo Area. It was strongly believed that a confined aquifer or semi-confined aquifer which its existence cause the water rushed out to the surface and formed a ponding area. The water seems to flow to lower area and formed several ponding within the site. It was reported by the locals that some of the resident in Petobo are using a tube well for a domestic water supply by punching through an aquifer zone in this area. At the time of puncturing a tube well, approximately between 5 and 10 meter height of water torrent appeared above ground surface [15]. This is another evidence that there is confined aquifer in Petobo Area. Figure 4a and 4b show the source of water and water ponding on the affected site of Petobo and a typical of tube well for domestic water supply.

(a) (c)

(b) (d)

Fig. 4 – Post Earthquake Site Survey in Petobo Site (a) Water Sources to Believe to Come Out from The Broken Aquifer (b) Typical of Tube Well For Domestic Water Supply (Widodo et al., 2019) (c) Occurrence of Landslide (d) Documentation of Liquefaction-induced Ground Failure (Sengara et al, 2019)

To assess the subsurface conditions and better understand the behavior of the site, subsurface exploration was carried out in several liquefied sites. Soil investigation was supported by Research Center for Disaster Mitigation-Institut Teknologi Bandung, join collaboration with PUSGEN, Department of Public Work, Indonesia.

The groundwater table post-earthquake measured varied from existing ground surface to 13.20 m below the existing ground surface. The observation shown that the groundwater in hilly area was deeper than coastal area. However, there were no monitoring wells installed in all sites before the earthquake, the initial groundwater table is not known.

Some soil samples, at Petobo, Jono Oge, Sibalaya, Balaroa and Sigi were collected and different laboratory tests were conducted. The grain size distribution at five area are quite similar with clay and silt content of approximately 10-30% 50-90% sand, and 0-25% gravel. According to the laboratory test data, most of the soil at all the sites were potentially liquefiable to most liquefiable soils. Figure 5 displays the grain size distribution curve results and criteria gradations of liquefiable soils in proposed area. The red and

blue line represent the boundary of criteria gradations of potentially liquefiable and most liquefiable soils, respectively (Tsuchida, 1970). The value of Specific Gravity varies in all sites between about 2.50 to 2.66.

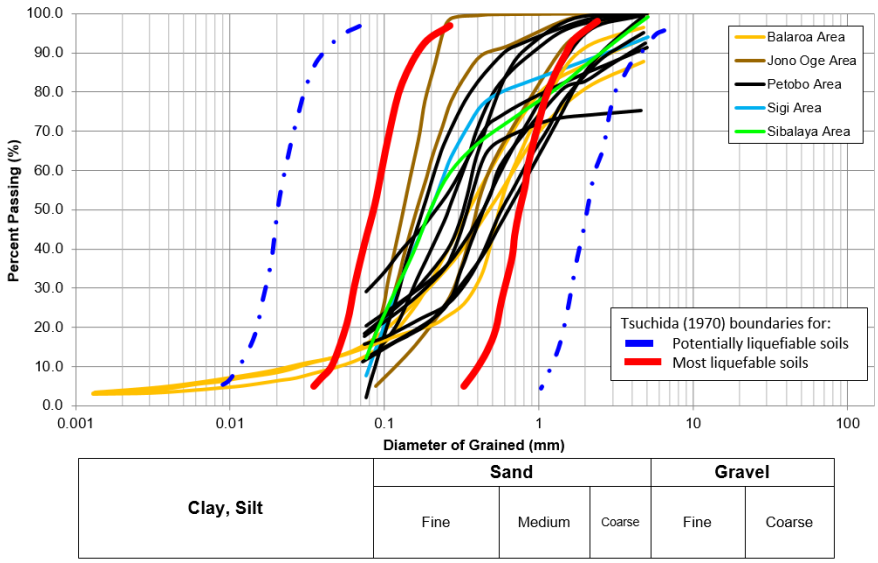

Fig. 5 – Grain Size Distribution Curve in Proposed Areas

Recognizing difficulties associated with in situ testing of granular soils, only the field (uncorrected) values of the SPT were used in this investigation. These SPT values provide a measure of the densities of the granular soils and allow comparison of the observations made from this case histories with those from other case histories on similar granular soils.

At Petobo site, the field investigation showed that the subsurface soil of the investigated area consists predominantly of silty sands to gravelly sand. In general, the uppermost layer consist of very loose to loose sand with a thickness about 7 meter and followed by medium sand layer until 17 m depth. The bottom layer is very dense layer with SPT values of more than 50 blows/30cm. Layer of clay and silt are found between a depth 14 to 25 m, they only appear to be lenses. SPT Values from all boreholes at Petobo site shown in Figure 6.

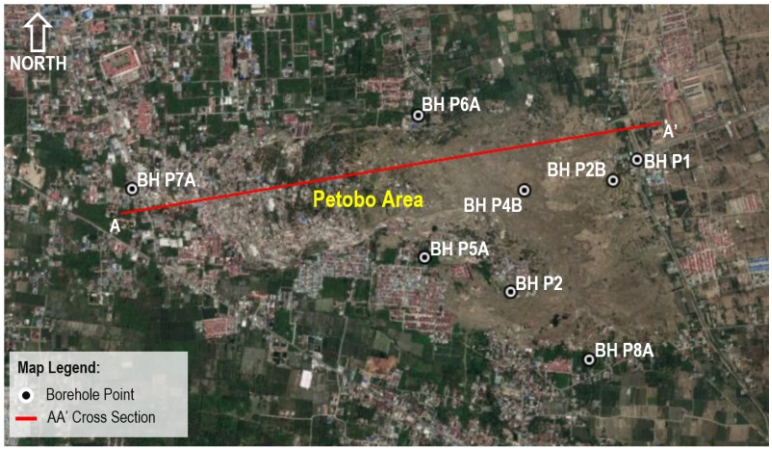

Fig. 6 – Drilling Positions in Petobo Site

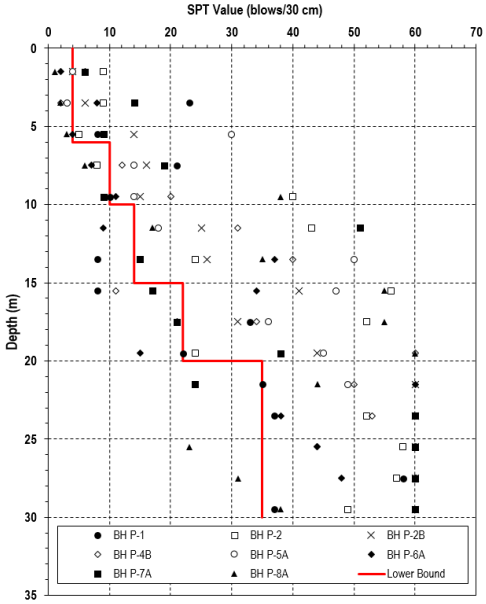

Fig. 7 – SPT Values at Petobo Site (Replotted from Promisco, 2019)

In addition, before earthquake the topographical condition are relatively flat with slope 1.3 – 5.4% (average slope is 2.3%). The topographical cross section AA' at Petobo area before earthquake event observed from Google Earth is shown in Figure 8.

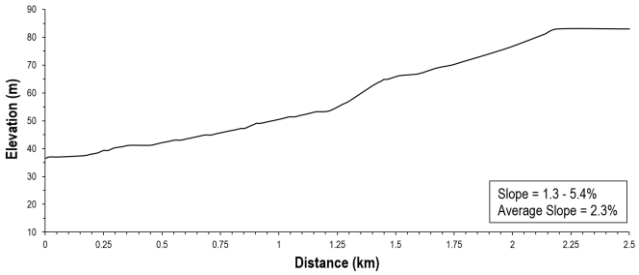

Fig. 8 – Topographical Section AA' Pre-Sliding Condition at Petobo Area (Replotted from Google Earth)

5. Coupled Effective Stress Analysis

Version 7.0 of the commercial computer program FLAC (Itasca Consulting Group, Inc. 2000) was used to perform the liquefaction occurrence back analysis of the Petobo Site due to Palu Earthquake. This program uses a two-dimensional finite difference formulation that models as a collection of plane strain elements. FLAC solves the dynamic stress-deformation problem using an explicit time stepping approach. This scheme is well suited to nonlinear evaluations and estimates of large deformations. FLAC also includes the ability to model groundwater flow using a finite difference formulation of seepage-consolidation. This capability was used to estimate the initial pore-water pressures as well as pore-water flow during earthquake shaking.

The analysis was performed using the built-in capabilities of FLAC as well as the user-defined constitutive models UBCSAND (Byrne et al., 2004) [2]. The UBCSAND model is a coupled (kinematic hardening) effective-stress model in plane-strain conditions. It uses an elasto-plastic formulation based on an assumed hyperbolic relationship between stress ratio and plastic shear strain. The model is capable of capturing the stiffness pre-liquefaction stage, the onset of liquefaction at the appropriate number of cycles, and very much softer post-liquefaction response as observed in cyclic simple shear-constant volume tests.

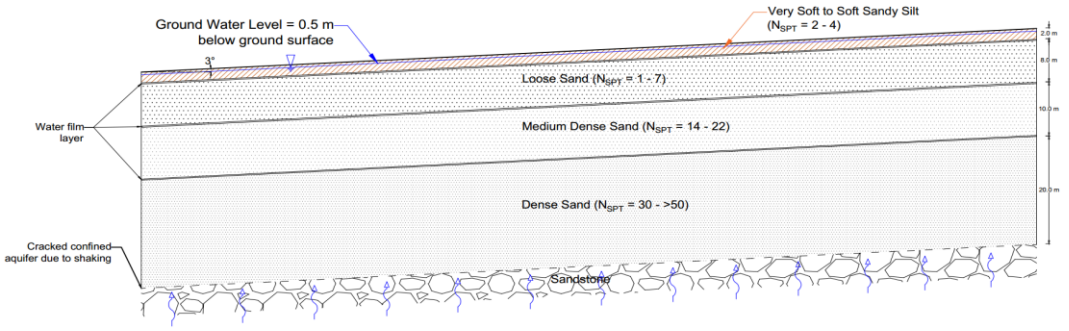

Fig. 9 – Illustration of Subsurface Condition in Petobo

Figure 9 shows the illustration of subsurface condition in Petobo. A combination of high water table, water film at every alteration layer, cracked confined aquifer and very loose to loose sand was thought to be the cause of the liquefaction. This illustration will be analyzed adopting following parameters:

- A cross section A-A' at Petobo site in Fig. 8, it was based on topographic data in Google Earth before earthquake event. This topographic covered the aerial extent of drilling test at Petobo site.
- In the absence of direct measurement of soil modulus and shear strength parameters, the input parameters for UBCSAND model were based primarily on the generic input parameters. These parameters provide a reasonable engineering estimate of the stiffness, the generation of pore pressures due to cyclic loading, and the post-liquefaction stress-strain behavior. The selected parameters were estimated from available SPT and soil classification data.
- Additional aquifer pressure of 100 kPa were applied at the base of the model. This pressure in accordance with the latest information of water torrent which has been discussed earlier at the time of puncturing a tube well for water supply.
- Combination of vertical and horizontal ground motion recordings from the PCI-PALU (BMKG-JICA) Stations.
- The UBCSAND model includes a hysteretic damping in its formulation, so it was not necessary to assign additional hysteretic damping. Additionally, a minor amount of Rayleigh damping 0.2% was used at dominant frequency of approximately 0.3 Hz to facilitate convergence and stability.

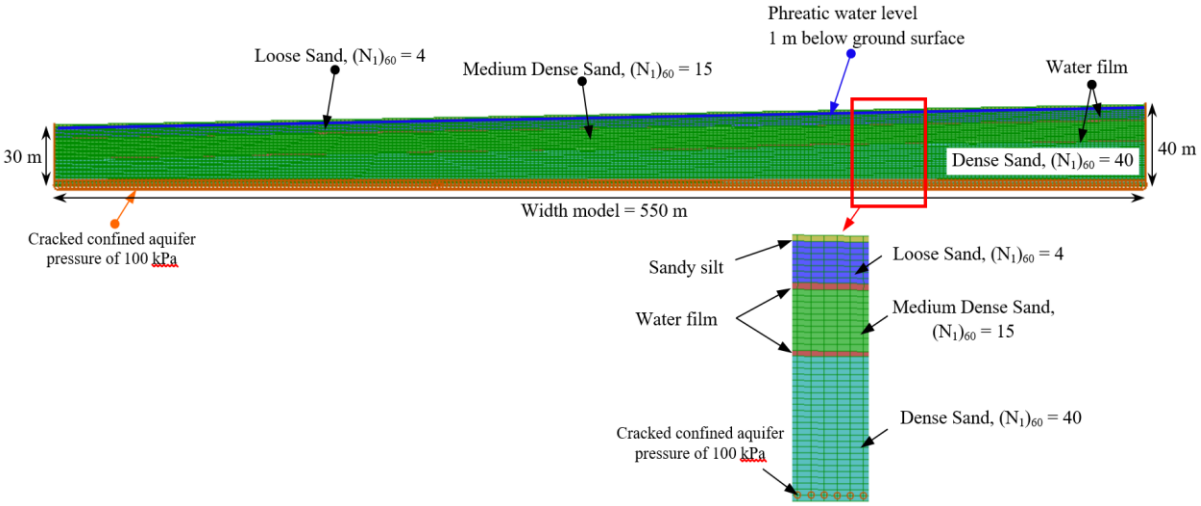

Fig. 10 – The Finite Difference Mesh used in The Analysis

Table 1 –Soil Parameters used in The Analysis using UBCSand Constitutive Model

Material	$(N_1)_{60}$	γ (kN/m^3)	c' (kPa)	ϕ' (deg)	kg_e	kb	m_e	n_e	Rf	n_p
Very Loose to Loose Sand	4	16.5	0	29	425	1277	0.5	0.5	0.85	0.4
Medium Dense Sand	15	17	0	33	790	1711	0.5	0.5	0.8	0.4
Dense Sand	40	18	0	42	1911	2548	0.5	0.5	0.75	0.4

Note: (1) $(N_1)_{60}$ = Normalized SPT values to 1 atm and 60% blow count energy
(2) γ = Bulk density
(3) kg_e & k_b = Shear and bulk modulus number
(4) m_e & n_e = Shear and bulk modulus exponent
(5) Rf = Failure ratio

The static equilibrium state at the time of the earthquake event is established to obtain the initial shear-stress distribution of the soil mass. The mechanical boundary conditions were used for static loading: the bottom of the model was fixed in both the vertical and horizontal directions, while the left and right edges of the model were fixed in the horizontal direction. The simple Mohr-Coulomb model with stress-dependent stiffness properties was also considered appropriate.

Several modifications were made to the model to convert it from the static analysis to the dynamic analysis, i.e., the changes in boundary conditions and soil constitutive. The base of the finite-difference grid was assumed to be complaint-base boundary to allow the absorption of the downward-propagating waves reflected from the surface. Quiet boundary conditions are applied at the base of the model to absorb the reflecting waves from the surface. In order to do this together with the application of earthquake motion at the base, the earthquake input motion must be applied as a stress boundary. Otherwise the effect of the quite boundary will be nullified when the input is applied as acceleration or velocity wave.

In the explicit-solution procedure, solution stability shall be considered. A time step that is smaller than some critical time step must be chosen. The calculation formula for critical time step of the triangular element is:

$$\Delta t_{crit} = \frac{A_z}{L_d}\sqrt{\frac{\rho}{K + \frac{4}{3}G}}$$

where, A_z represents the area of mesh element, and L_d the length of its diagonal. In other words, the maximum stable time step for dynamic analysis is determined by the largest material stiffness and the smallest mesh in the model. In this study, the minimum critical time step is 1.1×10^{-3}s while the calculated time step of 6.2×10^{-4}s which is estimated by the software itself. The critical time step is calculated using the mesh model which has 45 vertical columns and 275 horizontal layer. Typical mesh width are about 2 m while mesh heights are about 0.5 m. The average element size was chosen to implement the solution stability and to facilitate the transmission of the high-frequency (short wavelength) shear waves induced by the applied ground motion. Figure 10 demonstrates the FLAC mesh with rectangular and triangle shapes for this two-dimensional analysis.

The automatic rezoning logic is applied in the analysis to correct for severely distorted mesh conditions developed during the simulation of earthquake shaking. Additionally, an algorithm was defined that computes the excess pore pressure ratio, r_u, and stores the maximum value of r_u experienced by each element to determine whether or not an element liquefies. The displacement and excess pore pressure development at several points of interest such as at the toe, body, and crest of the slope (e.g, point 1, 2 and 3 in Figure 10) were monitored during the application of the Palu Earthquake.

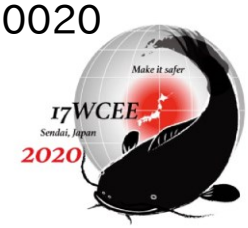

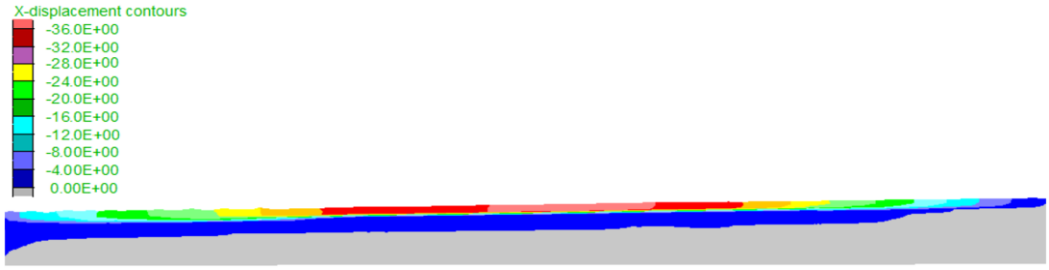

Fig. 11 – Contours of lateral displacement due to Palu Earthquake at Petobo Site with displacement in excess of 36 m

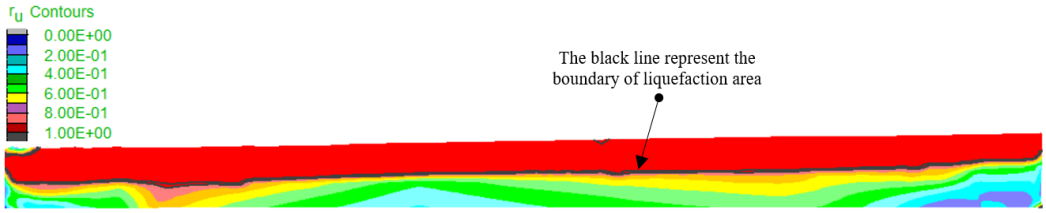

Fig. 12 – Contours of pore-pressure ratio (r_u) due to Palu Earthquake at Petobo Site. Pore pressure ratio of 1.0 indicates zones of liquefaction

The numerical results clearly show the high vulnerability of Petobo to seismic slope instability. Figure 11 illustrates the contours of maximum lateral deformation at the end of earthquake (93 seconds) with displacement in excess of 40 m occur on the toe until the body of the slope. The contour of excess pore-pressure ration equaling 1 (onset of liquefaction) at 93 seconds is also displayed in Figure 12. The liquefaction is likely to occur along the slope to a depth of 14 m. The zone of liquefaction appears to be increasing in thickness toward to the toe of the slope. The lateral displacement of the slope likely keep deform with time without any sign of stabilizing. The post-earthquake analysis is carried out to calculate the deformation until stabilization reached at approximately of 1000s.

The increase of pore-pressure quickly raises of 1.0 (liquefied) at about 18 – 19 seconds. However, the development of pore-pressure below 18 sec showed unclearly. This coincide with the characteristics of the acceleration and velocity pulses. The input ground-motion prior to 16 seconds have a little impact to the development of pore-pressure as the acceleration is relatively low (< 0.05g). The trend of increasing pore-pressure at several location of interest points tend to be similar. The values of r_u tend to be stable when reached r_u = 1 until the end of the earthquake even though the released energy getting smaller. Lateral displacement start to increase at about 20 seconds from the beginning of the earthquake and deform gradually until the energy of the earthquake is dissipated. Time histories of lateral displacement and excess pore-pressure development are presented in Figure 13 and Figure 14, respectively.

The debris flow run-out has been successfully modeled to resulted deformations in excess of 40 meter at the end of shaking and keep deform in the post-dynamic with a maximum displacement of about 90 meter at time duration of 1000sec. The shape of deformation curve versus time shows that lateral deformations keep increasing as a function of time in excess of 1000sec. This corresponds to the observed extremely large lateral deformation of flow liquefaction and gentle slope failures to cause lateral deformation of several hundred meters. The general magnitude and distribution of lateral displacement at post-liquefaction resulted from analyses compared to the deformation observed by satellite is reasonable. The slightly different of lateral displacement between the analysis and observation could be affected significantly by the magnitude of cracked confined aquifer pressure, non-linear soil behavior, and soil behavior at post-earthquake. However, the results obtained from the coupled effective stress analysis can be a useful insight for a safety evaluation of a slope which is susceptible to liquefaction.

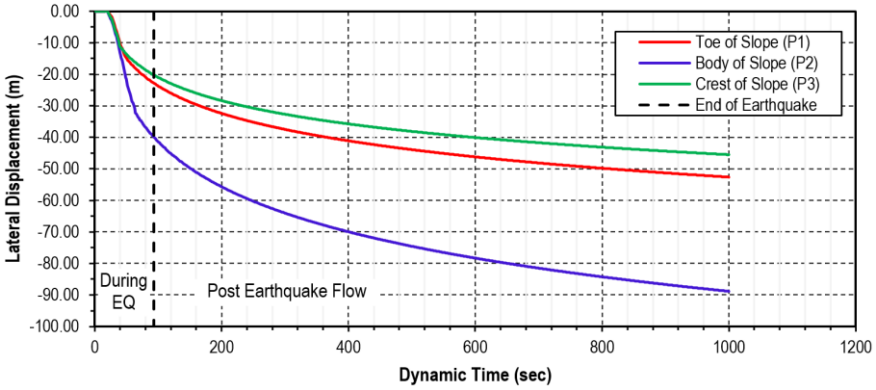

Fig. 13 – Time History of Lateral Displacement due to Palu Earthquake in several points interest during Earthquake and Post-Earthquake

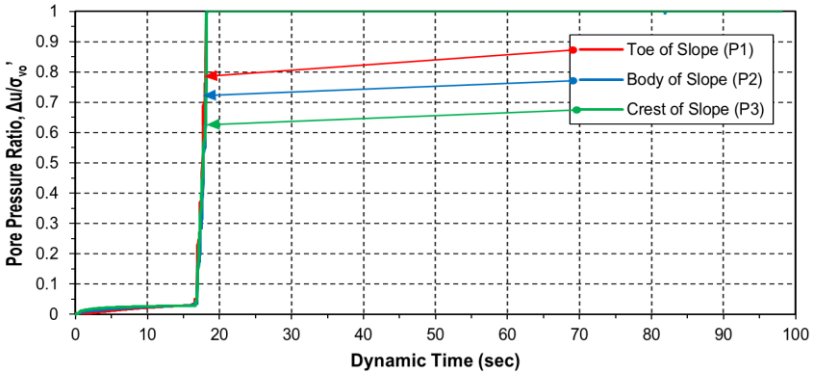

Fig. 14 – Time History of Excess Pore Pressure Ratio due to Palu Earthquake in several points interest during Earthquake

6. Concluding Remarks

An alternative approach for estimating deformations, pore-water pressures, and the degree of liquefaction under seismic loading has been described and demonstrated. The analyses is based on effective stress approach and incorporates modern numerical analysis techniques. Numerical modelling using FLAC utilizing UBCSAND constitutive model showed that the liquefaction occurrence has been verified and the results are presented in the form of deformations, settlements, and pore-water pressures development due to the earthquake.

A nonlinear effective stress-based approach coupled with aquifer pressure input has been applied to the slope at Petobo Area that experiences liquefaction-induced flow failure. The model's capability is demonstrated by comparing the numerical simulations with the deformation estimated satellite observation. The debris flow run-out analysis deform in excess of 40 meter at the end of shaking and keep deform in the post-dynamic with a maximum displacement of about 90 meter at time duration of 1000sec. The shape of deformation curve versus time shows that lateral deformations keep increasing as a function of time in excess of 1000sec. This corresponds to the observed extremely large lateral deformation of flow liquefaction and gentle slope failures to cause lateral deformation of about 250 meters.

It is observed that the numerical simulation models reasonably well the dynamic behaviour of the slope phenomenon large deformations failure. Therefore, the modelling techniques and its applicability is considered to be representative to the failure occurrences. The conducted liquefaction analysis could be applied for liquefaction potential analysis in supporting reconstruction design process as well as new design

of buildings and infrastructures in Palu city and surrounding areas. Moreover, the method could be applied for both post-earthquake evaluations and for pre-earthquake vulnerability predictions at others areas.

7. Acknowledgement

The authors would like to thank the Asahi Glass Foundation and the Research Institution and Community Services of Bandung Institute of Technology (LPPM-ITB) for Asahi Glass 2019 and P3MI 2020 research funding. The authors also appreciate the soil investigation data and earthquake ground motions data provided by Research Center for Disaster Mitigation, Institut Teknologi Bandung, JICA, and Department of Public Work. Appreciation to Mr. Yanmart Nainggolan and Krisman Nainggolan for the supports during site visit and data collection in Palu.

8. References

[1] Beaty, M.H. and Byrne, P.M. (2011). UBCSAND constitutive model: Version 904aR. Documentation Report: UBCSAND Constitutive Model on Itasca UDM Web Site.

[2] Byrne, P. M., Park, S.-S., Beaty, M.H., Sharp, M., Gonzalez, L., and Abdoun, T. (2004). Numerical Modeling of Liquefaction and Comparison with Centrifuge Tests. Canadian Geotechnical Journal, 41(2): 193-211. doi:10.1139/t03-088.

[3] Byrne, P. M. (1991). A Cyclic Shear-Volume Coupling and Pore-Pressure Model for Sand, Proceedings: Second Int. Comt. On Recent Advances in Geotechnical Earthquake Engineering and Soil Dynamics, St. Louis, Paper No.1.24, 47-55.

[4] Fang, J., Xu, C., Wen, Y., Wang, S., Xu, G., Zhao, Y. and Yi, L. (2019), The 2018 Mw 7.5 Palu Earthquake: A Supershear Rupture Event Constrained by InSAR and Broadband regional Seismograms. Remote Sens. 2019, 11, 1330; doi:10.3390/rs11111330.

[5] Hanifa, R. (2018). GEER – HATTI – PUSGEN Joint Survey on Palu Earthquake 2018 (M7.4) 13-18 Nov 2018. Presentation, Indonesian Ministry of Research, Technology and Higher Education, Jakarta, Indonesia, November 12, 2018.

[6] Ishihara, K. (1996). Soil Behaviour in Earthquake Geotechnics. Oxford Engineering Science Series. Oxford University Press.

[7] ITASCA. (2007). Manual FLAC Version 7.0, ITASCA Company.

[8] Kramer, S.L. (1996), Geotechnical Earthquake Engineering. Prentice Hall, New Jersey.

[9] Long X., and Tjok K. (2013). Analyses of Seismic Slope Stability and Subsequent Debris Flow Modeling, Proceedings of the 18th International Conference on Soil Mechanics and Geotechnical Engineering No. 2217-2220.

[10] Mason, H, B., Gallant, A, P., Hutabarat, D., Montgomery, J., Reed, A, N., Wartman, J., Irsyam, M., Prakoso, W., Djarwadi, D., Harnanto, D., Alatas, I., Rahardjo, P., Simatupang, P., Kawanda, A. and Hanifa, R. 2019. Geotechnical Reconnaissance: The 28 September 2018 M7.5 Palu-Donggala, Indonesia Earthquake. Geotechnical Extreme Events Reconnaissance.

[11] Sengara, I. W. and Sulaiman, A. (2019). Liquefaction Analysis Adopting Effective Stress Method for Petobo Site Post M_W 7.4 Palu Earthquake. International Conference in Commemoration of 20th Anniversary of the 1999 Chi-Chi Earthquake, Taiwan.

[12] Stark, T., Beaty, M., Byrne, P., Castro, G., Walberg, F., Perlea, V., Axtell, P., Dillon, J., Empson, W. and Mathews, D. (2012). Seismic Deformation Analysis of Tuttle Creek Dam. *Canadian Geotechnical Journal*, 49: 323 – 343.

[13] Tim Pusat Studi Gempa Nasional (PuSGeN). (2018). Kajian Gempa Palu Provinsi Sulawesi Tengah 28 September 2018 (M7.4). ISBN: 978-602-5489-14-3.

[14] Tsuchida, H. (1970). Prediction and Countermeasure against Liquefaction in Sand Deposits, Abstract of the Seminar of the Port and Harbour Research Institute, Ministry of Transport, Yokosuka, Japan, pp. 3.1-3.33 (In Japanese).

[15] Widodo, L.E., Simangunsong, G. M., Iskandar, I. and Prasetyo, S., H. (2019). The Role of Confined Aquifer in The Escalation of Palu Liquidation due to The Palu Earthquake of September 28, 2018 - A Hypothesis. Proceedings: 4th Annual Meeting of Association of Indonesian Groundwater Experts, Bandung, Indonesia.

[16] Yegian, M. K., Ghahraman, V. G. and Harutiunyan, R. N. (1994). Liquefaction and Embankment Failure Case Histories, 1988 Armenia Earthquake, J. Geotech. Geoenviron. Eng., Vol. 120, No.3, Paper No. 4636, 581-596.